An Efficient Method for Dimensioning Magnetic Shielding for an Induction Electric Vehicle Charging System

Karim Kadem, Fethi Benyoubi, Mohamed Bensetti, Yann Le Bihan, Eric Labouré, Moustapha Debbou

Progress In Electromagnetics Research, Vol. 170, 153–167, 2021

An Efficient Method for Dimensioning Magnetic Shielding for an Induction Electric Vehicle Charging System

Karim Kadem[1, 2, 3*], Fethi Benyoubi[4], Mohamed Bensetti[1, 2], Yann Le Bihan[1, 2], Eric Labouré[1, 2], and Mustapha Debbou[3]

Abstract—Recently, the number of electric vehicles (EVs) is increasing due to the declining of oil resources and rising of greenhouse gas emission. However, EVs have not received wide acceptance by consumers due to the limitations of the stored energy and charging problems in batteries. The dynamic or in motion charging solution becomes a suitable choice to solve the battery related issues. Many researchers and vehicle manufacturers are working to develop an efficient charging system for EVs which is based on magnetic emissions to transfer power. These emissions must be evaluated and compared to limits specified by standards (in and outside the vehicle) in order to not cause harmful effects on their environment (humans, pets, electronic devices...). This paper presents an efficient method for modeling electromagnetic emission in near field and sizing a magnetic shield for a wireless power transfer (WPT) system for EVs. A model based on elementary magnetic dipoles is developed in order to obtain the same radiation as the real WPT coil. This model is used to size a magnetic shield which will be placed under the vehicle to protect human body from magnetic emissions. The obtained shielding plate allows to respect the standards of magnetic emission by bringing a decrease of 43 dB to the levels of magnetic fields. This approach is experimentally validated.

1. INTRODUCTION

Up to now, electric vehicles (EVs) are not very attractive to consumers even with many government programs. Poor cruise performances of EVs continue to be the primary reason that impedes their market penetration. Electric storage technology is the major problem of EV. It requires a battery with large energy density, long cycle lifetime, and low cost [1–3].

Dynamic Wireless Power Transfer (DWPT) charging system for EVs application is a solution to solve the battery related issues. The DWPT solution discussed in this paper is a resonant inductive power transfer, and it is based on magnetic resonance coupling between the transmitter and receiver coils [4, 5].

Recently, as the need for EV charging and technological progress has increased, the transferred power and charging distance have increased from a few millimeters to a few hundred millimeters for kilowatt power levels [6, 7].

However, dynamic inductive charging presents a great risk of electromagnetic emission, especially since this type of charging is done in an environment accessible to people and pets (roads, garages, car parks...). It is therefore essential to study the electromagnetic radiation of this type of devices.

In this paper, the authors focus on the respect of the magnetic field (MF) emission standards of the wireless power transfer (WPT) systems. After a first stage of evaluation, the authors concentrate

Received 19 March 2021, Accepted 27 April 2021, Scheduled 11 May 2021

* Corresponding author: Karim Kadem (Karim.kadem@vedecom.fr).

[1] GeePs — Group of Electrical Engineering-Paris, Université Paris-Saclay, CentraleSupélec, CNRS, Laboratoire de Génie Electrique et Electronique de Paris, Gif-sur-Yvette 91192, France. [2] Sorbonne Université, CNRS, Laboratoire de Génie Electrique et Electronique de Paris, Paris 75252, France. [3] Institut VEDECOM — 23 bis Allée des Marronniers, Versailles 78000, France. [4] Laboratoire CEM, École Militaire Polytechnique (EMP), BP 17, Bordj el Bahri, Algiers 16111, Algeria.

on a more in-depth study on low frequency magnetic shielding. The aim is to pre-dimension a shielding plate which attenuates the MF emitted by the coupler and thus, to respect the limitations in terms of magnetic emission, not only in the environment of the vehicle but also inside the vehicle.

To carry out this pre-dimensioning, different measurements of the magnetic near field emission of a WPT coil will be presented. From these measurements, an equivalent dipolar radiation model can be built in order to obtain the same radiation as the real WPT coil. Such models based on magnetic dipoles can easily be implemented for analytical shielding studies. Several experimental tests will validate the proposed approach.

2. DYNAMIC WIRELESS POWER TRANSFER

The WPT solution explored in this study relies on the magnetic resonant coupling between the primary ground coil and the secondary vehicle coil. A typical WPT charging system scheme for EV is shown in Figure 1.

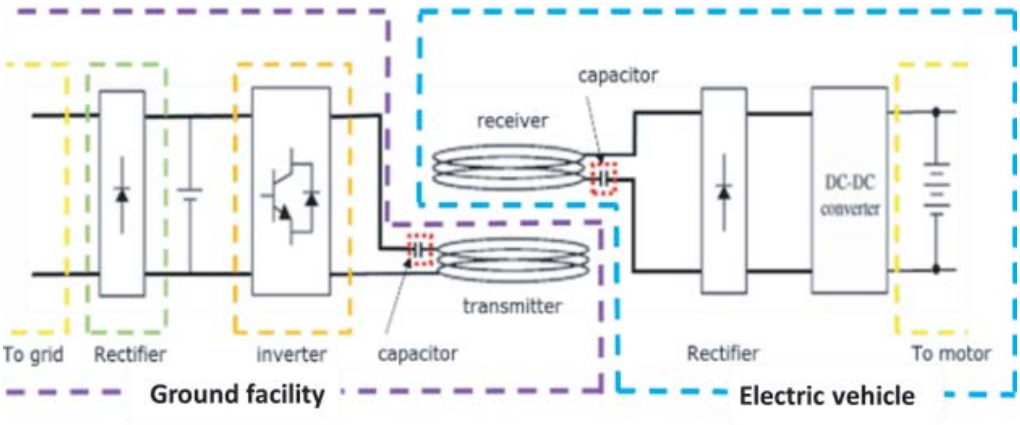

Figure 1. Typical WPT charging system for EVs [8].

The power of the AC grid is firstly converted to a direct current (DC) using an AC/DC rectifier. Then, the obtained DC power is converted into a high frequency AC power to feed the transmitting coil through a compensation network. The compensation network reduces the reactive power if the system operates at the resonance frequency close to 85 kHz, fixed by the standards.

The high frequency current in the primary coil generates an alternating magnetic field, inducing an AC voltage in the receiving coil. The obtained AC transferred power is rectified and transferred to a DC/DC converter to charge the EV battery.

The studied system during these research activities concerns a DWPT designed for a rated power of 2.5 kW. It feeds a RENAULT Twizy car. This system is shown in Figure 2(a), while Figure 2(b) shows the primary pad (coil + ferrite). This WPT system is defined as WPT1-Z1 class (according to the standard J2954 corresponding to a power level lower than 3.7 kVA, and a coil air gap lower than 150 mm) [9].

The main specifications of charging system are summarized in the following Table 1.

3. EMISSION EVALUATION

In the case of a WPT system, the possible effects of magnetic radiation on biological tissues as well as electromagnetic compatibility (EMC) problems are of prime importance. They must be addressed at the design stage, because the system generates a strong, predominantly magnetic electromagnetic field. This problem is even more pronounced in the case of dynamic WPT, where the vehicle is charging while in use and therefore, in an environment accessible to people and pets (interior, areas around the vehicle, etc.). This represents a significant risk of exposure to high levels of magnetic radiation.

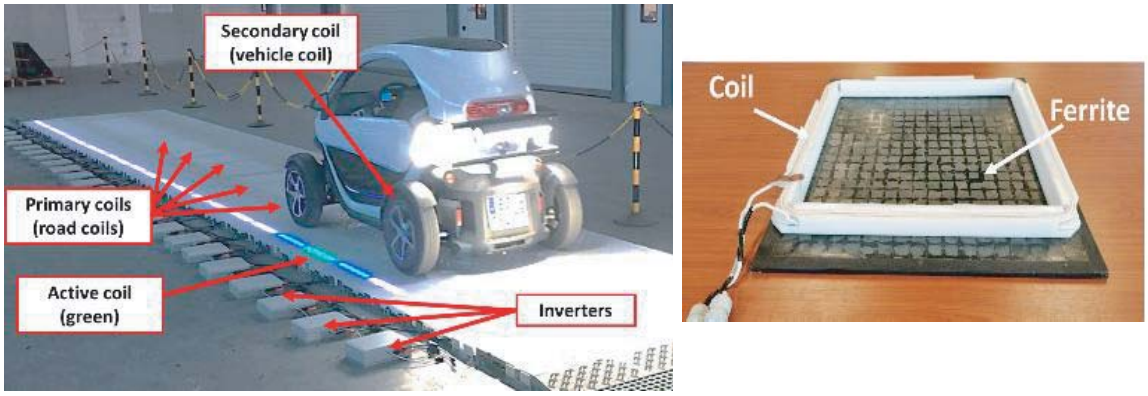

(a) (b)

Figure 2. (a) Experimental bench of dynamic induction charging of an electric vehicle, (b) WPT Coil [10].

Table 1. Parameters of the VEDECOM WPT system.

Parameter	Value
Transferred Power	2.5 kW
DC input voltage	60 V
Coupling coefficient	0.1 to 0.3
Coil turns number	6
Primary and secondary inductances	63 µH
Primary and secondary resonant capacitor	56 nF
Primary-secondary Airgap	150 mm
Inverter switching frequency	80 kHz–90 kHz
Coils dimensions	468 mm × 468 mm × 13 mm
Ferrites dimensions	500 mm × 600 mm × 2 mm
System efficiency	92%

Several standards such as IEC 61980 [11], SAE J2954 [9], ISO 19363 [12], and even the IEC 63243 [13] (standard concerning the DWPT which is being drafted) deal with emission problems. All these standards refer to ICNIRP 2010 [14] for the level of recommended field. These ICNIRP 2010 levels are 27 µT (RMS) today (for the WPT system frequency range) and will surely be more tolerant with the release in 2020 of a new report from ICNIRP (2020) [15]. In France, these emission questions are treated by the INERIS, a national organization, which is still referring to the ICNIRP 98 [16] values. (6.25 µT RMS or 8.8 µT Peak). All these standards consider not only the radiated field in the vehicle but also near it to limit the exposure of people or animals in the vicinity of the latter.

The first part of this work concerns magnetic field evaluation. The aim of this study is to predict the magnetic induction that can permeate inside the passengers compartment of the vehicle.

Figure 3 shows the levels of the magnetic induction in a plane located at a height of 284 mm above the primary coil without the vehicle chassis. We are therefore "virtually" inside the EV. This study was carried out using COMSOL software, which allows finite element method (FEM) simulations for the rectangular coils previously seen. The primary coil is supplied with a peak current $I_{peak} = 60$ A at 85 kHz.

We notice that the ICNIRP 98 recommendations were exceeded inside the vehicle ($B_{peak} = 8.8$ µT). However, note that the vehicle chassis is absent while it participates in shielding the magnetic field.

Two actions can be considered for reducing magnetic radiation in the passenger compartment in

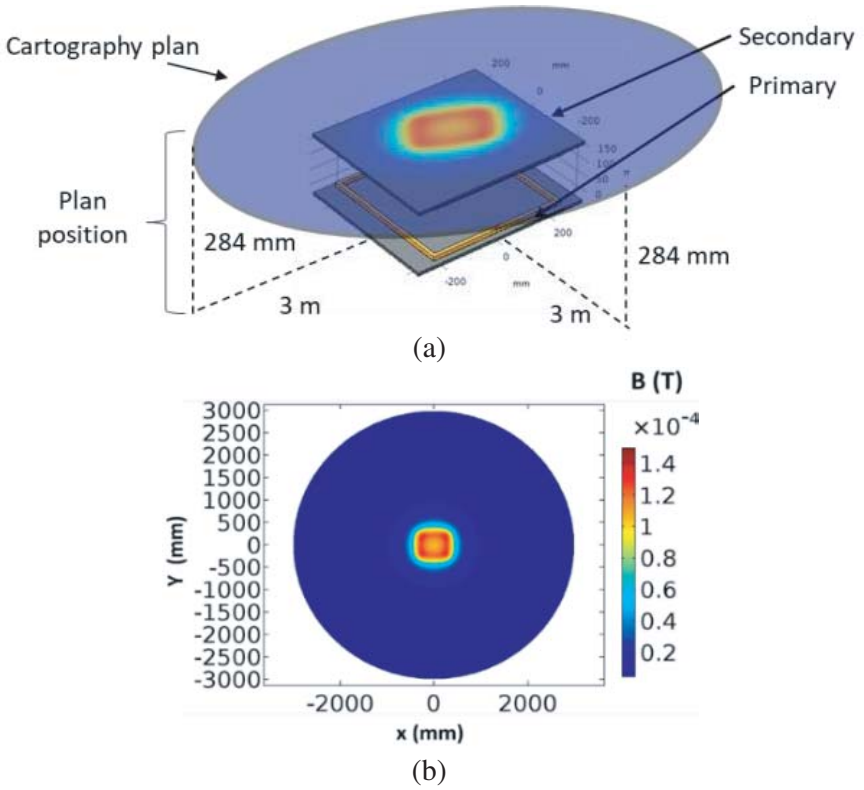

Figure 3. Cartography of the magnitude of magnetic induction standard, (a) position of the mapping plane, (b) magnetic induction on the mapping plane.

order to meet the limitations of the ICNIRP. One can either reduce the current in the coil and therefore the transferred power or consider implementation of magnetic shielding.

This last solution is preferred and required in a real system as it offers a higher power transfer capability. In the next section, we present an approach allowing to analytically pre-dimension such magnetic shielding.

4. EMISSION MODELING AND MAGNETIC SHIELDING

The proposed equivalent dipole method makes it possible to overcome the problems arising from FEM method in free space as it involves large mesh size. This method is based on replacing the excitation source (coil + ferrite) by a set of equivalent dipole sources giving substantially the same radiation as the real magnetic source. This approach is illustrated in Figure 4.

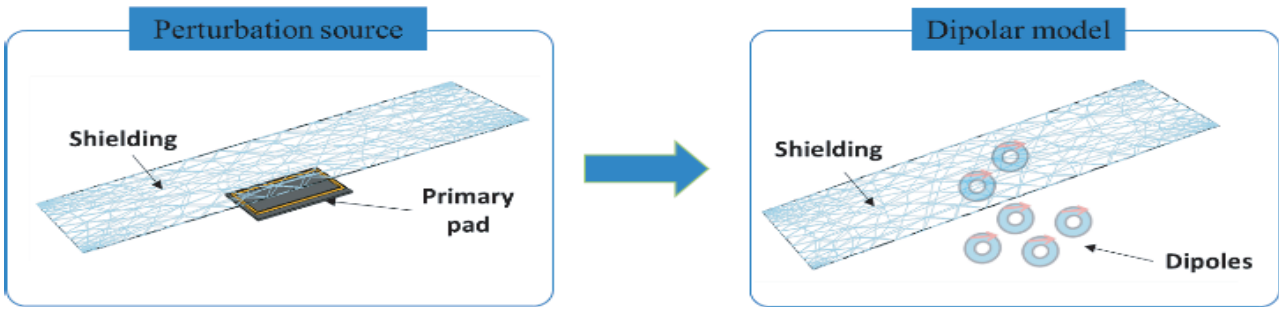

Figure 4. Adopted approach.

In what follows, we choose to ignore the presence of the secondary pad (secondary coil and its ferrite plate) and therefore, to size the shielding in the most restrictive configuration in terms of radiation. In fact, the ferrite plate of the secondary helps reducing the magnetic field into the passenger compartment. Moreover, this choice is justified because it will take into consideration the dynamic aspect of the system, where a transmitting coil cannot directly face the secondary coil, or even, for example, in the case of a vehicle not equipped with a WPT system which passes over the primary coil.

The magnetic shield dimensioning approach implemented can be broken down into two steps. Figure 5 shows these two steps. In the first step, the radiation source (transmitting coil with ferrite plate) is replaced by equivalent sources (elementary dipoles) to give radiation close to that of the original source. The construction of this model is obtained from measurements of the magnitude of magnetic field in the near field area. Note that it could also be carried out from the results of a 3D numerical simulation.

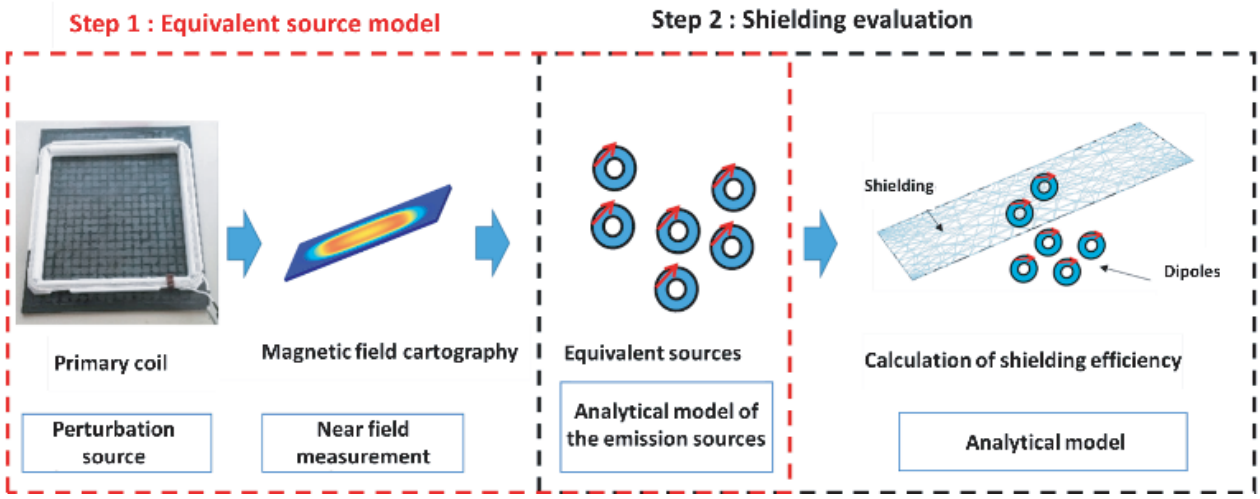

Figure 5. Adopted approach for the prediction of shielding effectiveness.

Secondly, the elementary sources will be used to analytically determine the effectiveness of magnetic shielding for given shielding screen parameters.

4.1. Dipolar Model

Several approaches exist which allow to recreate the electromagnetic field radiated by a source of disturbance, especially for small power electronics boxes [17–19]. In this paper, a dipole-based method is chosen [20, 21]. This approach is initially designed for the EMC studies of power electronics boxes. We make an extension of this method for an automotive system where several problems can be encountered, like the size of the field of study, the dispersion of the arrangement of dipoles, scale problems, and even the high value levels of the magnetic field.

To model the coil emission, magnetic field measurements should be done. These near field measurements were obtained by using a near field test-bench (Figure 6) based on a robotwith3translation axes and one rotation. The robot moves a magnetic probe (MP) over the primary coil and its ferrite (at a height of 0.1 m) with high precision. This MP is generally composed of a conductive loop, which generates a voltage from the varying magnetic flux. A computer controls the robot and acquires data from a spectrum analyzer. Data corresponding to the three components of the magnetic field emitted by the WPT coil leads to three magnetic field maps (cartographies).

Following the approach proposed in [18], a magnetic dipole distribution is determined to replace the WPT coil by an equivalent source giving a very similar magnetic field distribution (Figure 7).

This model is found by minimizing a fitness function using a genetic algorithm combined with a pattern search algorithm [18].

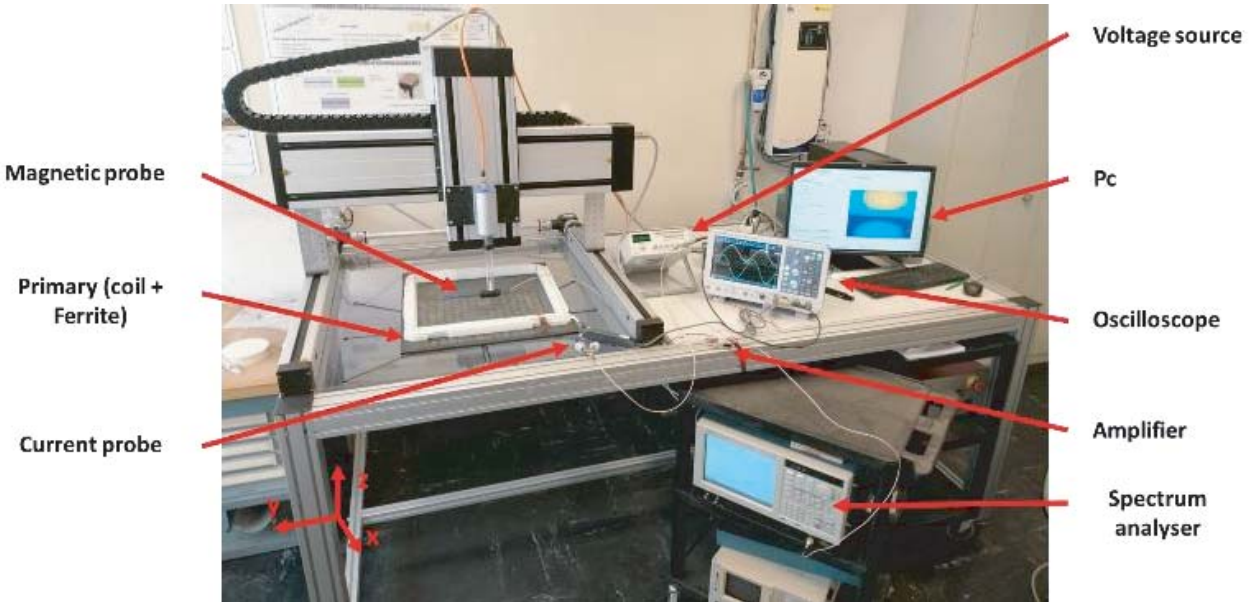

Figure 6. Near field bench.

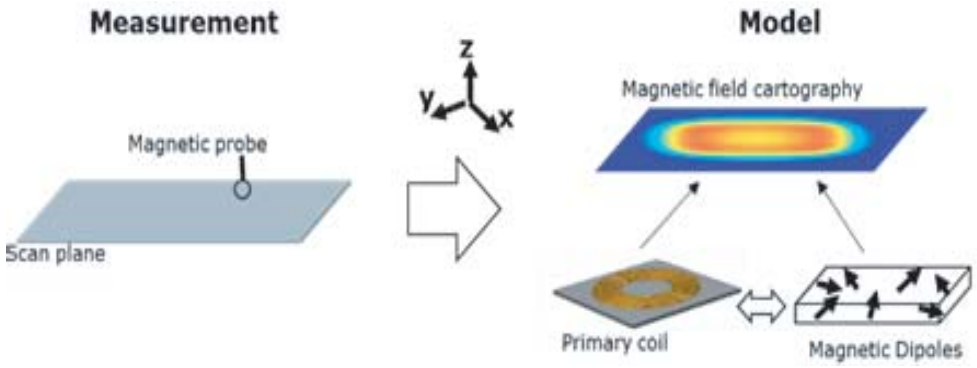

Figure 7. Principle of a radiated model construction.

First, the magnetic field measurements are done at low current value (125 mA). These measurements (with measurement error less than 1.5%) are compared to the WPT coil FEM model simulation obtained by COMSOL (Figure 8).

After this first step of FEM validation (with an error of less than 5% between measurement and COMSOL model), the cartography (map) obtained at 60A (the system rated current) is used to generate the dipolar model which allows to find the number, location, and components of the dipolar model moments.

In the following paragraph, the steps used by the developed algorithm to determine the equivalent dipolar model are presented.

The radiated magnetic field generated by a set of dipoles can be written as follows [18]

$$|H| = |PM| \tag{1}$$

where:

H: Magnetic field vector $(3i \times 1)$;
i: Number of measurement points;
M: Dipole moments vector $(3n \times 1)$;
P: Matrix depending on the position of dipoles $(3i \times 3n)$;
n: Number of used magnetic dipoles in the model;

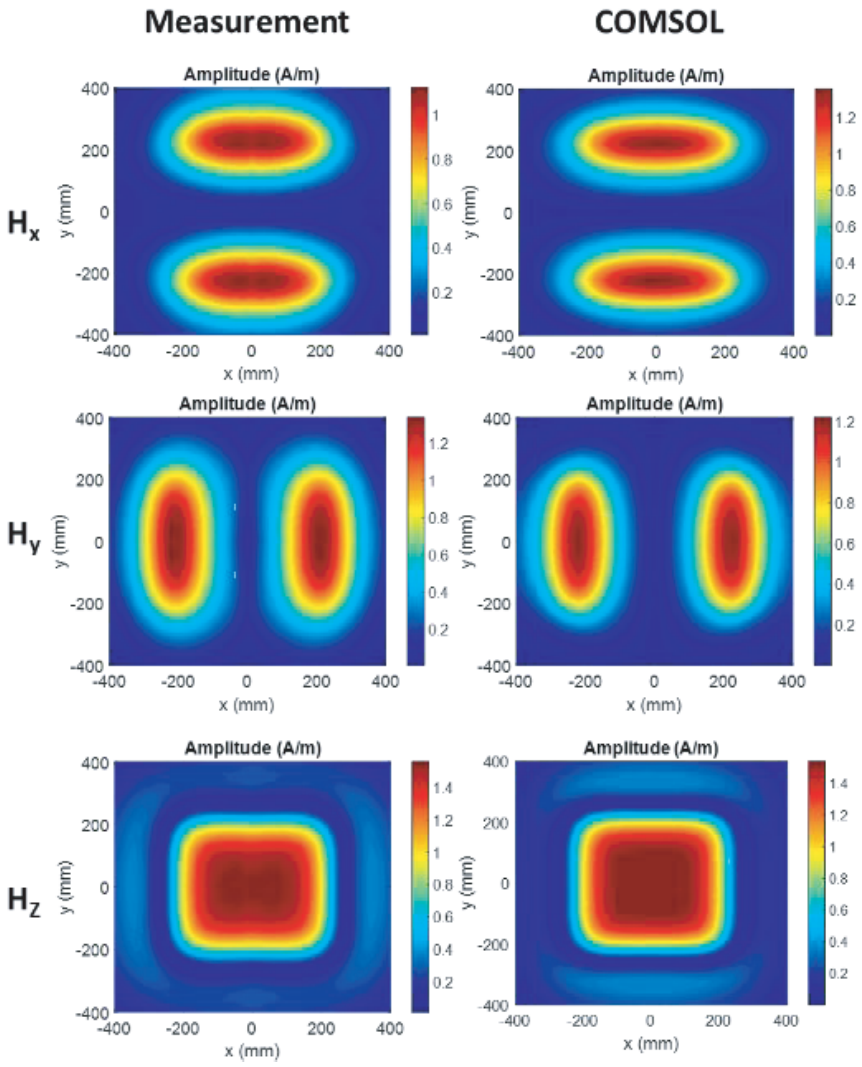

Figure 8. Comparison between measurements and COMSOL results.

$|x|$: Vector containing the magnitude of the elements of the vector x.

The factor "3" is due to the three components of the magnetic field at a spatial location.

Figure 9 shows the optimization algorithm used to find the number, the position, and the moment of the dipoles. Δf is defined as the difference between the fitness function calculated in two consecutive numbers of dipoles.

The fitness f is defined by:

$$f = \sqrt{\frac{\sum \left(|(H_{xm} - H_{xs})|^2 + |(H_{ym} - H_{ys})|^2 + |(H_{zm} - H_{zs})|^2 \right)}{\sum \left(|H_{xm}|^2 + |H_{ym}|^2 + |H_{zm}|^2 \right)}}$$

where "m" represents the measured values and "s" the dipolar model simulated values.

First, we determine the initial parameters (dimension of the search area, maximum number of dipoles, and the height of the measurement plane). Secondly, the optimization algorithm is used to find only the positions of dipoles (reduced number of unknown parameters). Then, the moments are deduced by a matrix inversion. In addition, this method looks for the dipoles in a finite volume, which leads to finding a reduced number of unknowns.

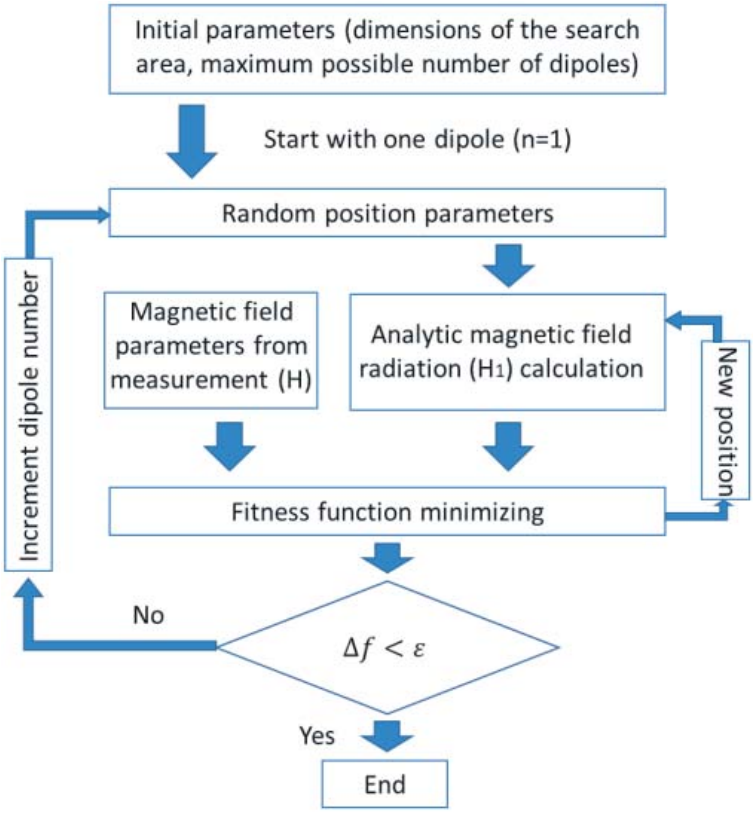

Figure 9. Optimization algorithm.

In this example, a model composed of 15 magnetic dipoles is obtained, and the fitness function is equal to 2.3% at a frequency of 85 kHz. The algorithm takes 1907 s to find the solution (position and dipole moments).

Figure 10 shows a comparison between the COMSOL results and the dipolar model. This comparison is made on a plane located at a height of 100 mm above the primary coil.

In Figure 11, we compare the values of the magnetic field H on the line at $x = 0$ mm (the black lines illustrated in Figure 10).

We can notice a good agreement between the COMSOL model and the dipolar model for the three components of the magnetic field (H_x, H_y, H_z). However, to quantify the comparison results, the feature selective validation (FSV) tool is used. The FSV algorithm has been developed to compare any two sets of data and put them in an objective and comprehensible form. This tool was conceived as a technique to quantify the comparison of data sets by mirroring the perceptions of engineers [22, 23].

The application of FSV to the validation of data is a key element in a current IEEE Standard. This tool makes possible to estimate the validity of the used model by comparing its results with the simulations. The structure of the compared data can be a vector or a matrix. This tool is based on the separation of real or complex data to be compared in two groups: the first one analyzes the difference of amplitude (Amplitude Difference Measure, ADM); the second analyzes the difference between the signal characteristics (Feature Difference Measure, FDM). The range of values for ADM and FDM is Excellent (Ex), Very good (VG), Good (G), Fair (F), Poor (P), and Very poor (VP) [24].

Figures 12, 13, and 14 show the ADMc (Amplitude Difference Measure confidence histogram) and the FDMc (Feature Difference Measure confidence histogram) for the three components of the field H.

Different shielding plates made of different materials were used and compared. Characteristics of these shielding plates are shown in Table 2.

Figure 19 shows data obtained from analytical calculations and measurements. The shielding effectiveness is represented as a function of the frequency and is evaluated for the 4 types of shielding

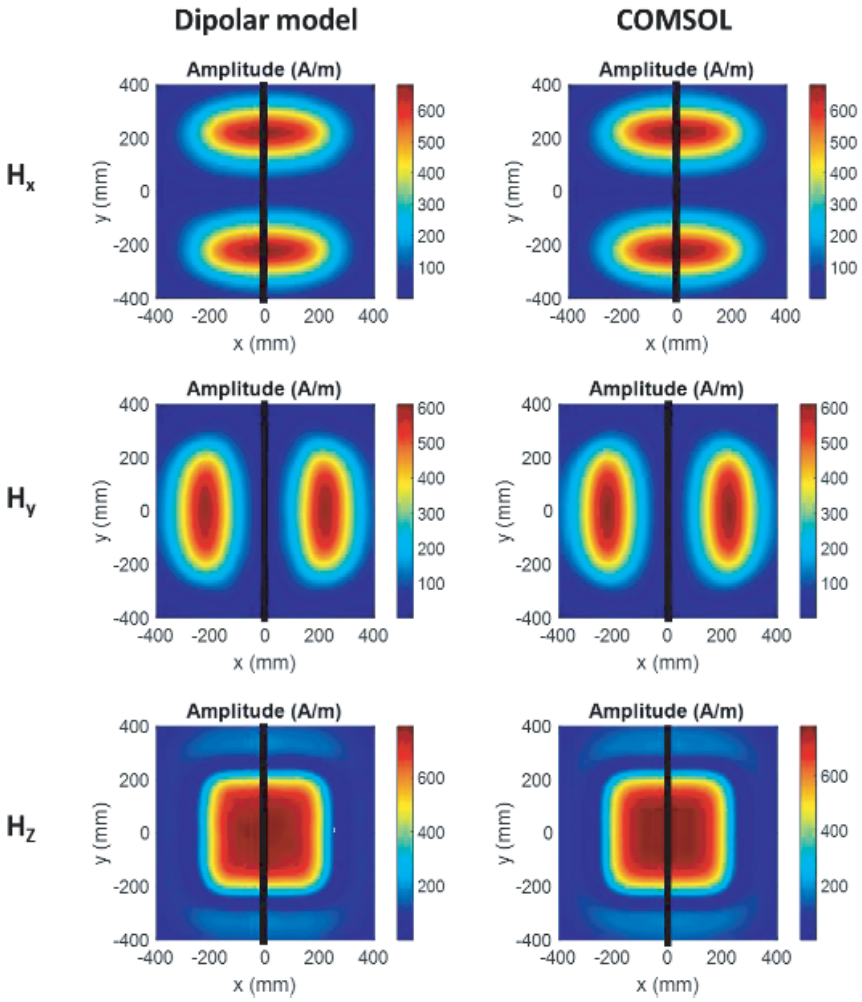

Figure 10. Comparison between the COMSOL results and the dipolar model.

Table 2. Characteristics of the shielding plates.

	Material type	Conductivity (MS/m)	Thickness (mm)	Size (mm × mm)
Plate 1	A5 (95% aluminum)	35	0.1	800 × 800
Plate 2	A5 (95% aluminum)	35	0.2	800 × 800
Plate 3	AG3 (50% aluminum)	18.8	1	800 × 800
Plate 4	AG3 (50% aluminum)	18.8	1.6	800 × 800

plates. Frequencies range from 1 Hz to 100 kHz. The distance between the coil and the shielding plate is 18 mm, and the sinusoidal current feeding the coil is $I_{peak} = 0.45$ A.

The results of the comparison between COMSOL results and model obtained results are good in general for the three components of the magnetic field.

This model is going to be used instead of the real WPT primary coil for the analytical determination of the shielding.

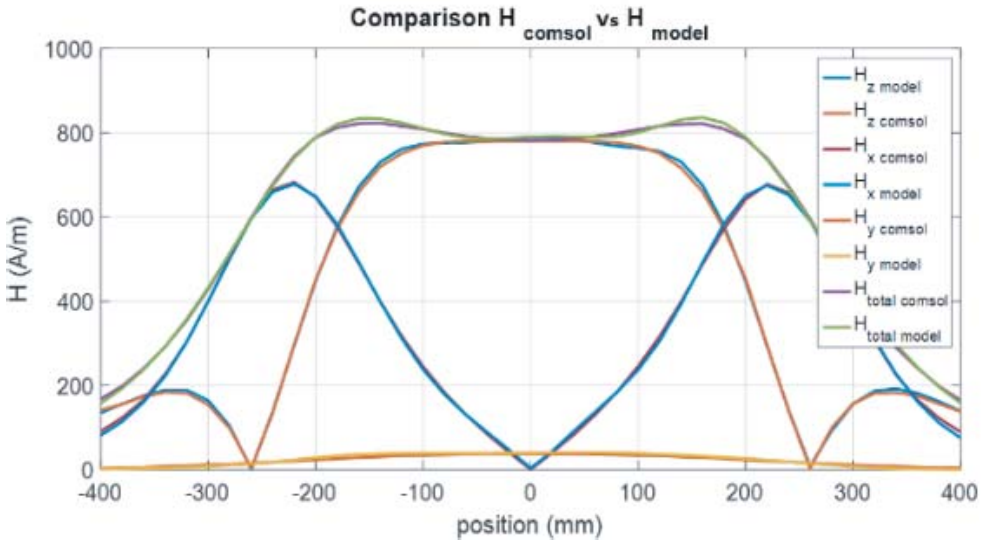

Figure 11. Comparison between the COMSOL results and the dipolar model along the $x = 0$ axis.

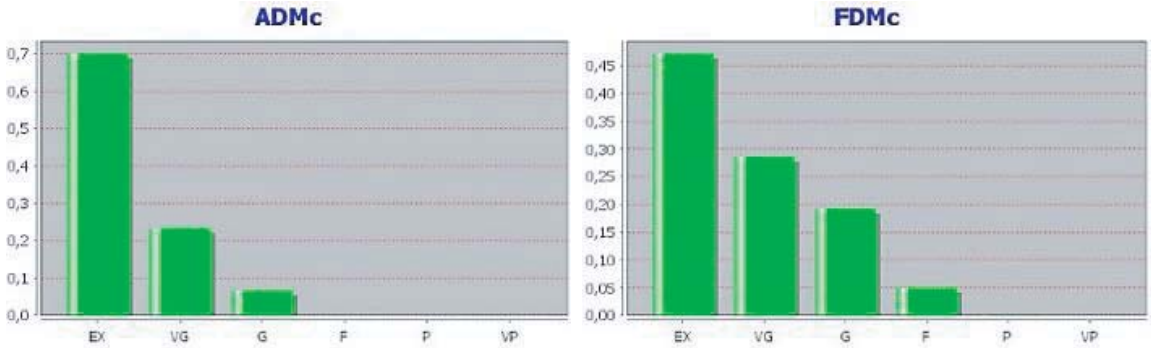

Figure 12. ADMc and FDMc for the component H_x.

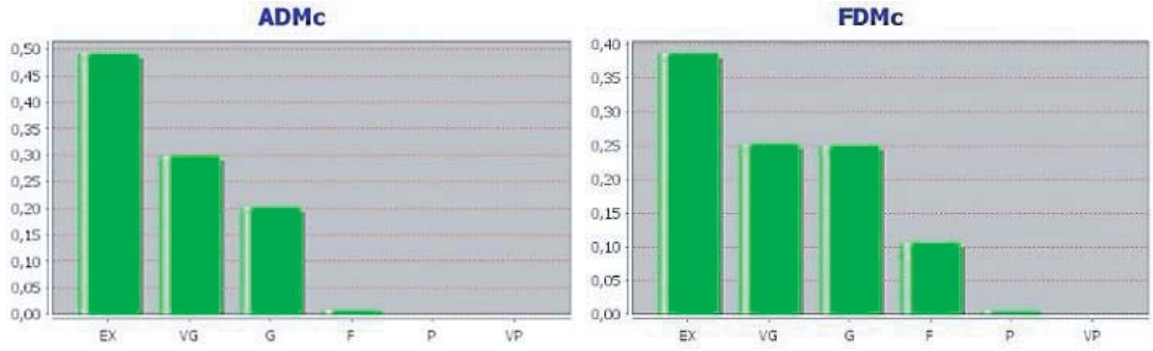

Figure 13. ADMc and FDMc for the component H_y.

4.2. Shielding Effectiveness

The magnetic shielding efficiency (SE_H) is defined as being equal to the attenuation of the magnetic field amplitude provided by a shield. It quantifies the performance of a shielding [25–27].

$$SE_{H\,\mathrm{dB}} = 20 \log \frac{\|H_{WTOS}\|}{\|H_{WS}\|} \tag{2}$$

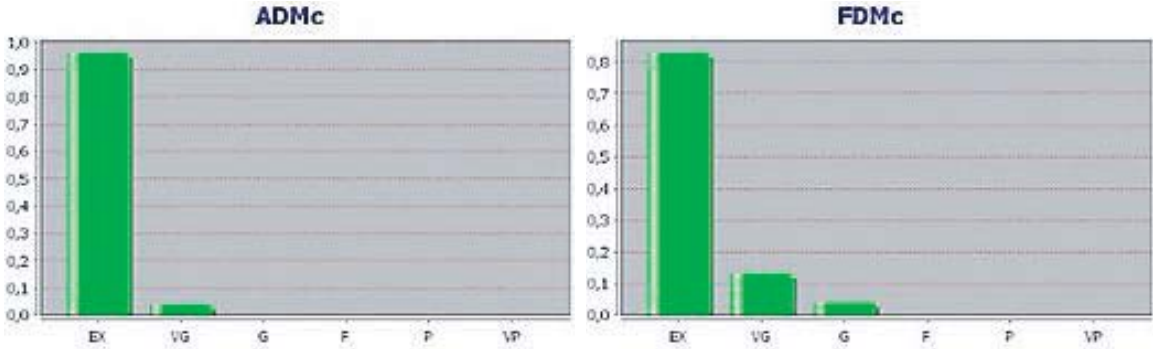

Figure 14. ADMc and FDMc for the component H_z.

where:

H_{WTOS}: magnetic field without shielding plate.

H_{WS}: magnetic field with shielding plate.

The different mechanisms that contribute to the effectiveness of shielding generate three types of field attenuation commonly referred to as "losses": the absorption losses, reflection losses, and multiple reflection losses [28, 29].

The shielding efficiency (SE) in decibels (dB) (see Equation (3)), for a shielding plate of very large lateral dimensions is expressed as the sum in dB of the three previous mechanisms(reflection, absorption and multiple reflection).

$$SE_{\text{dB}} = A_{\text{dB}} + R_{dB} + M_{\text{dB}} \tag{3}$$

where:

A_{dB}: represents the absorption loss (in dB) of the wave as it proceeds through the shield plate.

R_{dB}: represents the reflection loss (in dB) caused by field reflection on the shield surface.

M_{dB}: represents the additional effects of multiple reflections (in dB).

Magnetic induction simulations were performed on a line above the position where the shield will be located (inside the vehicle cabin). This line along the z axis is for coordinates $x = 0\,\text{mm}$, $y = 0\,\text{mm}$, $z = [181.5\,\text{mm}$ to $1800\,\text{mm}]$ ($z = 0\,\text{mm}$ corresponds to the level of the upper surface of the primary coil).

Figure 15 shows the 15 dipoles used, the position of the shielding plate, and the line on which the magnetic emissions are evaluated.

Figure 16 shows the magnitude of the magnetic induction radiated by all equivalent dipoles and simulated along the blue line in Figure 15 (unshielded).

The simulations show a high intensity of the magnetic induction near the chassis (20 cm above the ground) and a decrease of this field as one moves away from the source of disturbance. We also note an exceedance of up to 43 dB (600 µT (Peak) instead of 8.8 µT (Peak)) compared to the threshold imposed by the recommendations of the ICNIRP.

After having calculated the desired attenuation and using the shielding efficiency study approach presented above, we propose to reduce the magnetic field in order to comply with the recommendations of the ICNIRP by using a shielding plate of 0.1 mm thickness made of aluminum alloy (AG3). This plate has a shielding efficiency around 43 dB at 85 kHz. The choice of this type of material is justified by its competitive price compared to copper and by its mechanical strength compared to pure aluminum.

4.3. Experimental Validation

Experimental results are needed to validate the proposed model. The production of full-scale system is very heavy in terms of time and resources. Assuming the absence of saturation in ferrite plate, we can consider validating the results obtained previously by making coils with reduced size.

These miniature coils are obtained by making a scale model from the real size. This 1 : 10 scale miniaturization allows us to experimentally validate analytic results. The designed coils are built with

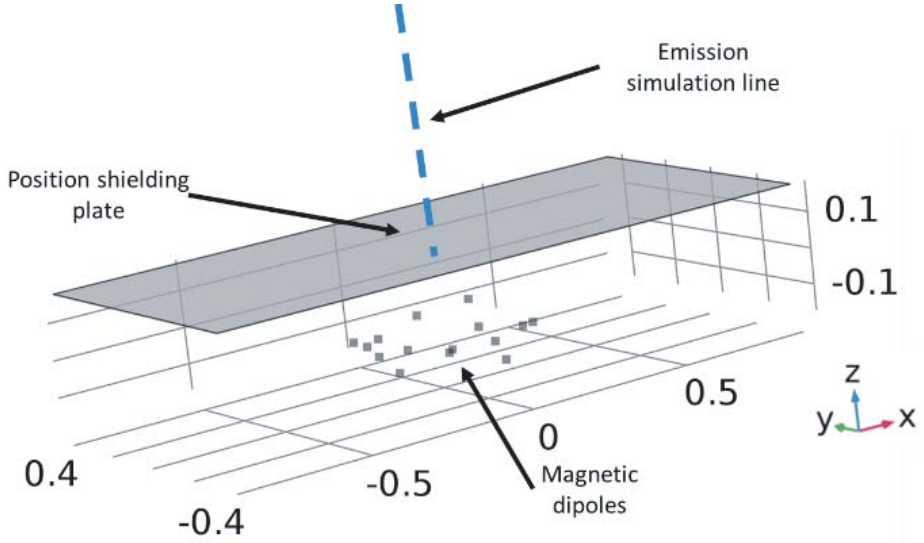

Figure 15. Set of dipoles, position of shielding plate and emission simulation line.

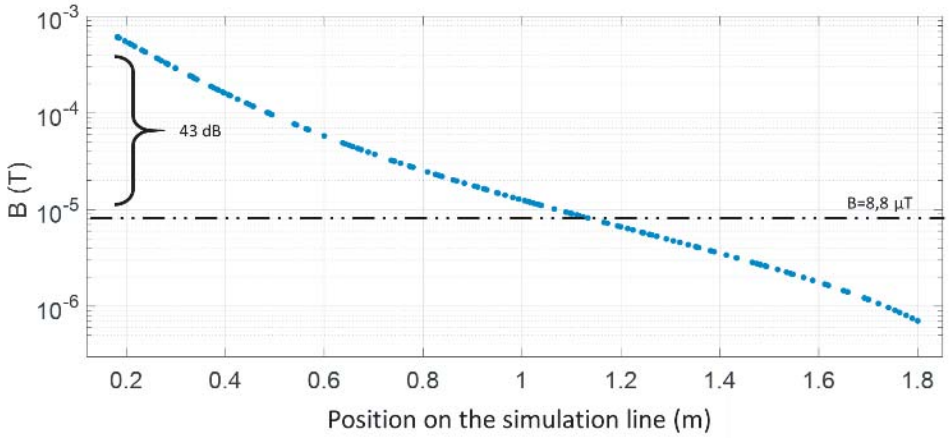

Figure 16. Magnitude of the magnetic induction radiated by the equivalent dipoles simulated on the line shown in the Figure 15.

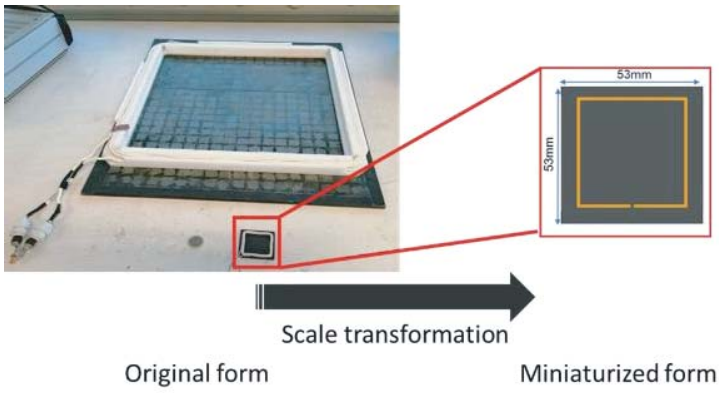

Figure 17. Miniaturized prototype made in the laboratory.

ferrite plates and Litz wire with the same number of turns (6). Figure 17 shows the coil of the full-size coupler and the corresponding miniaturized coil.

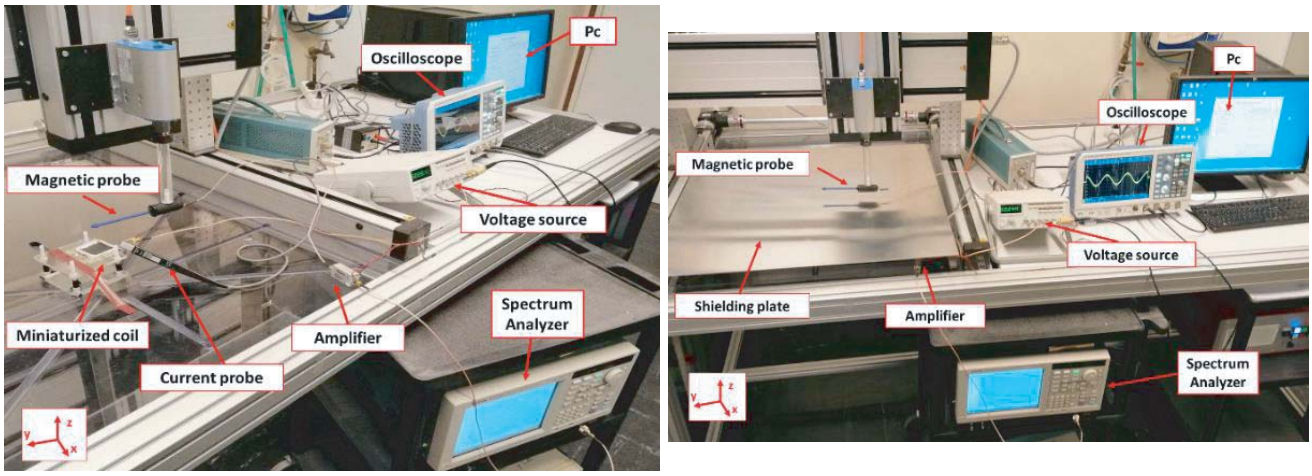

(a) (b)

Figure 18. Experimental validation bench. (a) Without shielding plate, (b) with shielding plate.

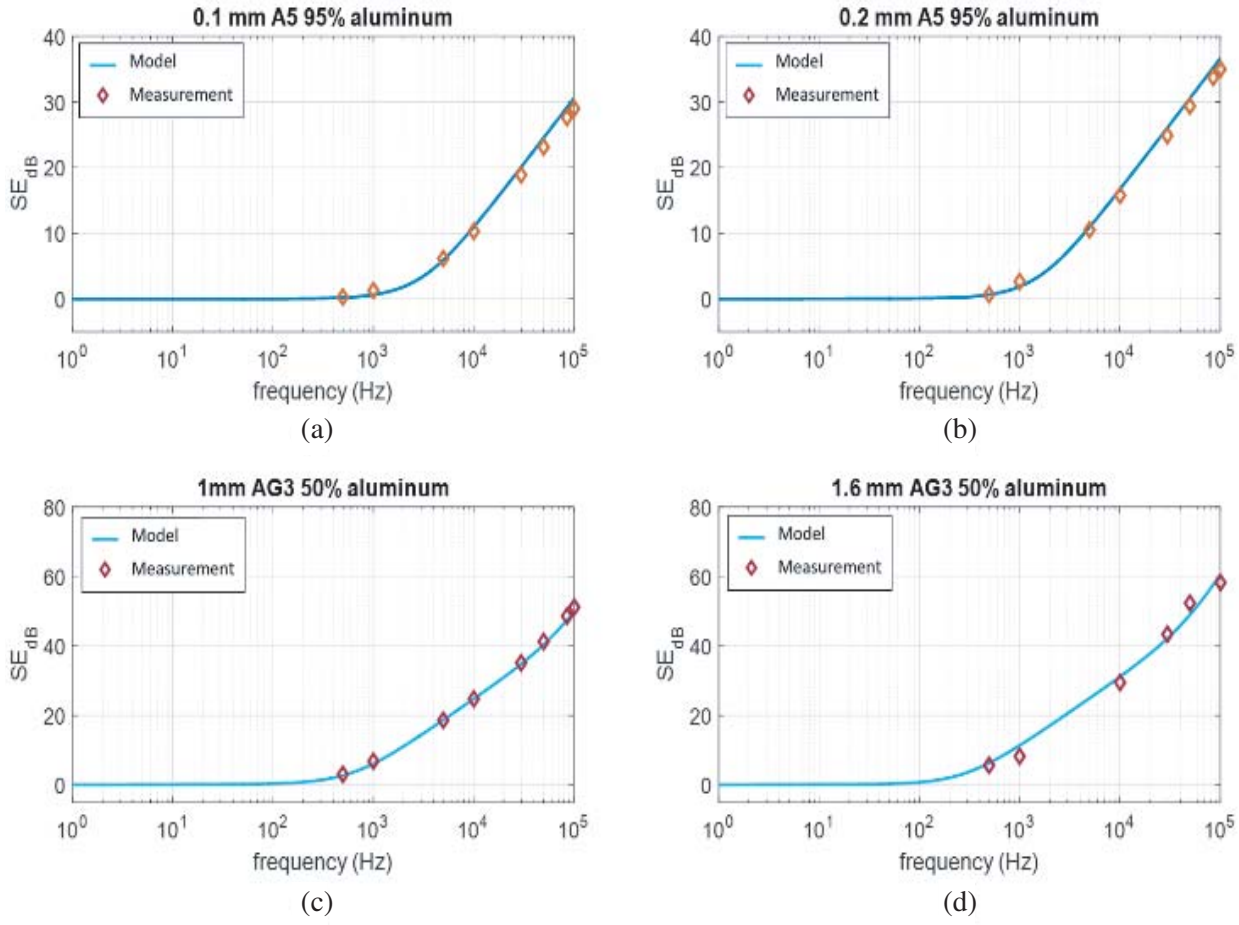

(a) (b) (c) (d)

Figure 19. Analytical and measurement shielding efficiency, (a) for Plate 1, (b) for Plate 2, (c) for Plate 3, (d) for Plate 4.

Figure 18 shows the experimental validation bench. This validation was carried out with the miniaturized coil.

Figure 19 demonstrates the high influence of the operating frequency, the thickness and conductivity of the material.

Furthermore, a good agreement between the analytical shielding efficiency values (obtained from the dipole model calculation) and measurement results is observed (with an error of less than 5%). Such results show that the analytical calculation of the shielding efficiency using equivalent dipoles is pertinent.

5. CONCLUSION

This paper is devoted to the study of near-field magnetic emissions of a WPT coil. It focuses more particularly on the study of an efficient method for modeling radiated emissions using equivalent dipoles. These dipoles are deduced from an optimization algorithm. The method has been experimentally tested and shows good agreement with measurements and those calculated with COMSOL.

We have also demonstrated that this model can be used to analytically calculate the field radiated by WPT systems and to size the shielding to be implemented to meet the standards. The use of the analytic model to evaluate shielding efficiency permits to get a fast and simple pre-dimensioning of the shielding plate.

All obtained results have been experimentally validated in laboratory using a near field test-bench.

REFERENCES

1. Coca, E., *Wireless Power Transfer Fundamentals and Technologies*, 2016.
2. Caillierez, A., P. A. Gori, D. Sadarnac, A. Jaafari, and S. Loudot, "2.4 kW prototype of on-road Wireless Power Transfer: Modelling concepts and practical implementation," *2015 17th European Conference on Power Electronics and Applications (EPE'15 ECCE-Europe)*, No. 1, 1–9, 2015.
3. Ruffo, R., V. Cirimele, M. Diana, M. Khalilian, A. La Ganga, and P. Guglielmi, "Sensorless control of the charging process of a dynamic inductive power transfer system with an interleaved nine-phase boost converter," *IEEE Trans. Ind. Electron.*, Vol. 65, No. 10, 7630–7639, 2018.
4. Caillierez, A., "Etude et mise en oeuvre du transfert de l'énergie électrique par induction: Application à la route électrique pour véhicules en mouvement," Thèse de doctorat, Université PARIS-SACLAY, 2016.
5. Boys, J. T., G. A. Covic, and A. W. Green, "'Stability and control of inductively coupled power transfer systems," *IEE Proc. — Electr. Power Appl.*, Vol. 147, No. 1, 37, 2000.
6. Covic, G. A., J. T. Boys, M. Budhia, and C. Huang, "Electric vehicles — Personal transportation for the future," *World Electr. Veh. J.*, Vol. 4, 693–704, 2010.
7. Budhia, M., G. Covic, and J. Boys, "A new IPT magnetic coupler for electric vehicle charging systems," *IECON Proc. (Industrial Electron. Conf.*, 2487–2492, 2010.
8. Kadem, K., F. Cheriet, E. Laboure, M. Bensetti, Y. Le Bihan, and M. Debbou, "Sensorless vehicle detection for dynamic wireless power transfer," *2019 21st European Conference on Power Electronics and Applications, EPE 2019 ECCE Europe*, 1–6, 2019.
9. SAE J2954, "Wireless power transfer for light-duty plug-in/electric vehicles and alignment methodology," *SAE Int.*, 2017.
10. Kadem, K., Y. Le Bihan, M. Bensetti, E. Laboure, A. DIET, and M. Debbou, "Reduction of the shielding effect on the coupling factor of an EV WPT system," *2019 IEEE PELS Workshop on Emerging Technologies: Wireless Power Transfer, WoW 2019*, 2019.
11. IEC 61980-1, *Electric Vehicle Wireless Power Transfer (WPT) Systems – Part 1: General Requirements*, 2019.
12. ISO 19363, "Electrically propelled road vehicles — Magnetic field wireless power transfer — Safety and interoperability requirements," 2018.

13. IEC 63243, "Interoperability and safety of dynamic Wireless Power Transfer (WPT) for electric vehicles," 2021.
14. Matthes, R., J. H. Bernhardt, A. F. McKinlay, and International Commission on Non-Ionizing Radiation Protection, *Guidelines on Limiting Exposure to Non-ionizing Radiation?: A Reference Book Based on the Guidelines on Limiting Exposure to Non-ionizing Radiation and Statements on Special Applications*, Vol. 74, No. 4. 1999.
15. ICNIRP, "Guidelines for limiting exposure to electromagnetic fields (100 kHz to 300 GHz)," *Health Phys.*, Vol. 118, No. 5, 483–524, 2020.
16. ICNIRP, "Guidelines for limiting exposure to time-varying electric and magnetic fields (1 Hz to 100 kHz) — International commission on non-ionizing radiation protection—," *Health Phys.*, Vol. 99, No. 6, 818–836, 2010.
17. Benyoubi, F., "Caractérisation en champ proche des émissions rayonnérs de boitiers de blindage électromagnétique," Thèse de doctorat, Université de Nantes, 2018.
18. Benyoubi, F., et al., "An efficient method for modeling the magnetic field emissions of power electronic equipment from magnetic near field measurements," *IEEE Trans. Electromagn. Compat.*, Vol. 59, No. 2, 609–617, 2017.
19. J. R. Regué, M. Ribó, J. M. Garrell, and A. Martín, "A genetic algorithm based method for source identification and far-field radiated emissions prediction from near-field measurements for PCB characterization," *IEEE Trans. Electromagn. Compat.*, Vol. 43, No. 4, 520–530, 2001.
20. Abdelli, W., A. Frikha, X. Mininger, L. Pichon, and H. Trabelsi, "Prediction of radiation from shielding enclosures using equivalent 3-D high-frequency models," *IEEE Trans. Magn.*, Vol. 51, No. 3, 1–4, 2015.
21. Tong, X., D. W. P. Thomas, K. Biwojno, A. Nothofer, P. Sewell, and C. Christopoulos, "Modeling electromagnetic emissions from PCBs in free space using equivalent dipoles," *Eur. Microw. Week*, No. 10, 280–283, 2009.
22. Orlandi, A., A. P. Duffy, B. Archambeault, G. Antonini, D. E. Coleby, and S. Connor, "Feature Selective Validation (FSV) for validation of Computational Electromagnetics (CEM). Part I — The FSV method," *IEEE Trans. Electromagn. Compat.*, Vol. 48, No. 3, 460–467, 2006.
23. Rajamani, V., C. F. Bunting, A. Orlandi, and A. Duffy, "Introduction to Feature Selective Validation (FSV)," *IEEE Antennas Propag. Soc. AP-S Int. Symp.*, Vol. 1, No. 1, 601–604, 2006.
24. Orlandi, A., A. P. Duffy, B. Archambeault, G. Antonini, D. E. Coleby, and S. Connor, "Feature Selective Validation (FSV) for validation of Computational Electromagnetics (CEM). Part II — Assessment of FSV performance," *IEEE Trans. Electromagn. Compat.*, Vol. 48, No. 3, 460–467, 2006.
25. Basyigit, I. B. and M. F. Caglar, "Investigation of the magnetic shielding parameters of rectangular enclosures investigation of the magnetic shielding parameters of rectangular enclosures with apertures at 0 to 3 GHz," *Electromagnetics*, Vol. 36, No. 7, 434–446, 2016.
26. Basyigit, I. B., M. F. Caglar, and S. Helhel, "Magnetic shielding effectiveness and simulation analysis of metalic enclosures with apertures," *2015 9th Int. Conf. Electr. Electron. Eng. (ELECO), Bursa, Turkey*, 328–331, 2015.
27. Feliziani, M. and S. Cruciani, "Mitigation of the magnetic field generated by a Wireless Power Transfer (WPT) system without reducing the WPT efficiency," *Int. Symp. Electromagn. Compat. (EMC Eur.*, 610–615, 2013.
28. Frikha, A., M. Bensetti, L. Pichon, F. Lafon, F. Duval, and N. Benjelloun, "Magnetic shielding effectiveness of enclosures in near field at low frequency for automotive applications," *IEEE Trans. Electromagn. Compat.*, Vol. 57, No. 6, 1481–1490, 2015.
29. Araneo, R. and S. Celozzi, "Exact solution of the low-frequency coplanar loops shielding configuration," *IEE Proc. — Sci. Meas. Technol.*, Vol. 149, No. 1, 37–44, 2002.